Websites:
http://www.sciencepub.net
http://www.sciencepub.net/rural

Emails:
editor@sciencepub.net
sciencepub@gmail.com

World Rural Observations

MARSLAND PRESS
Multidisciplinary Academic Journal Publisher

3-Dimensional Advanced Guidance Scheme for Lunar Descent and Landing

Ibrahim Mustafa Mehedi [1], Takashi Kubota [2]

[1.] Department of ECE, Faculty of Engineering, King Abdulaziz University, Jeddah 21589, Saudi Arabia
[2.] The University of Tokyo, Tokyo, Japan
imehedi@kau.edu.sa

Abstract: A 3-dimensional advanced guidance scheme is necessary to perform a successful precise lunar landing mission. This paper outlines a 3-dimensional comparison of different methods of solution of motion control equations for guidance scheme of lunar descent and proposes a 3-dimensional advanced solution that allows a full depiction for a descent vehicle motion from orbital states down to the final landing event. In the conventional 2-D methods of solution, some inadequate assumptions are exist limits the validity of the solutions. The proposed research allows a complete representation of the descent module motion from orbital speed conditions down to the final landing state.
[Ibrahim MM, Takashi K. 3-Dimensional Advanced Guidance Scheme for Lunar Descent and Landing. World Rural Observ 2021;13(4):29-41]. ISSN: 1944-6543 (Print); ISSN: 1944-6551 (Online). http://www.sciencepub.net/rural. 3. doi:10.7537/marswro130421.03.

Keywords: Advanced solution; 3-D modeling; Lunar landing

1. Introduction

Pinpoint landing technology is the most important technology for future space missions. To demonstrate this technology Moon is the suitable destination. Therefore, return to the moon become a demanding issue. A lot of scientists and engineers confirmed considerable interests in the past couple of decades [Cheng (1964), Cheng et al. (1966), McInnes (2003), Klumpp (1971), Ueno and Yamaguchi (1998), Sostaric (2006), Xing-Long et al. (2008) and Chao and Wei (2008)]. Safe landing capability is also essential, which can be achieved while a spacecraft land vertically and softly on the lunar surface[Kenji et al. (2002)]. Gravity-turn descent is one of the solutions for this purpose. This technique entails the lander thrust vector is oriented opposed to the velocity vector along complete flight path of the vehicle [McInnes (1999)]. Using inertial measurement unit, the information about the velocity vector can be identified to insert as an input of attitude controller that can maintain thrust vector parallel to the velocity vector instantaneously but in opposite direction. The great benefit of using gravity-turn descent is to have guaranteed upright landing, and fuel consumption is optimal [Cheng et al. (1966)].

The primary task of descent scheme is to solve the spacecraft 3-dimensional motion equations easily and efficiently, that will help to generate reference trajectory for lunar descent and landing. Conventional target trajectory generation schemes are numerically complex and cumbersome [Klumpp (1971), Klumpp (1974)]. The 2-dimensional full numerical solution of spacecraft motion equation is indeed a time consuming issue and not suitable for on-board real-time trajectory generation algorithm to achieve precise and safe landing. Therefore it is necessary to find a 3-Dimensional qualitative solution instead of numerical one. This paper proposed a 3-dimensional advanced solution scheme for lunar descent equations to circumvent complexity.

Solution of spacecraft motion equations in conventional gravity-turn descent is numerical and iterative in nature. This numerical method of solution limits the validity for real-time application because of complexity. Therefore, it is essential to solve the spacecraft motion equations analytically. Consequently some analytical solutions are available for a related problem [McInnes (1999)]. Suboptimal solutions are also discussed for Mars pin-point landing [Najson and Mease (2006), Topcu et al. (2007), Braun and Manning (2007), Lutz (2010), and Blackmore et al. (2010)]. It showed the comparisons between rigid body model and point mass of a Mars lander during powered descent phase. A convex optimization [Ackmese and Polen (2007)] has developed approximate solution to the powered descent guidance problem considering minimum-fuel constraint as a second order cone program (SOCP). Alternatively the same optimization problems can be solved in polynomial time using interior-point-method algorithms [Ye (1997), Sturm (1999) and Sturm (2002)]. In addition, the convex optimization is solved for real-time application in [Mattingley and Boyd (2010)]. More extensive comparisons of the convex optimization approach to alternative approach are available in [Steinfeld et al. (2010), Blackmore et al. (2010) and Acikmese and Blackmore (2011)]. However, nonlinear optimization is not guaranteed about the number of

required iterations to find a feasible trajectory and also not reliable to get the global optimum. Therefore, It is necessary to propose a purely analytical targeting solution to generate multi-dimensional trajectories "on-the-fly" or to re-target the spacecraft to another landing site altogether. At the end of last century, a purely 2-dimensional analytical solution is demonstrated for lunar landing mission[McInnes (1999)]. The similar 2-dimensional concept is proposed in [Chomel and Bishop (2009)] based on analytical solutions to the equations for downrange and altitude excluding cross range distance.

Apart from the Apollo solution, other researchers have proposed solution scheme for lunar descent equations. But the motion equations for spacecraft descent are solved in conventional way consists some limitations too. Because, in conventional solution lunar surface is imagined a plane flat surface and centrifugal acceleration term is ignored [Kenji et al. (2002), McInnes (1999), and Ueno and Yamaguchi (1998)]. Ignoring centrifugal acceleration term during lunar descent it considers a constant and vertical gravitational acceleration as only other force acting on the descent vehicle [McInnes (1999)]. This confines the vehicle to be landed precisely on the lunar surface. Moreover, since centrifugal forces are unnoticed, the conventional method of solution limits the validity to regimes where the descent vehicle velocity is very small relative to the local orbital velocity and therefore, it is only be used to describe terminal descent, when the vehicle has braked from orbital velocity and close to the lunar surface. Consequently the authors demonstrate a three dimensional advanced method of descent solution for a spherical homogeneous lunar surface where the centrifugal forces are retained and descent can be initiated from its orbital speed condition. In this paper, some logical values are examined to determine a better approximation for centrifugal acceleration term without ignoring it, but the gravity is assumed to be constant in magnitude. These assumptions are reasonable while the descent starts from vehicle's orbit. The proposed 3-dimensional advanced solution over conventional descent method allows a full representation of descent module motion from orbiting condition down to final vertical landing situation. To represent the significant improvement in the new solutions, 3-dimensional representation is shown for both three steps in this study and these are full integrated solution, conventional solution and advanced solution.

2. Scope of lunar guidance

After Earth-Moon transfer, lunar landing spacecraft can descend directly to the surface from the hyperbolic orbit, or the vehicle can first enter into a parking orbit around the Moon before attempting to start descent. Both direct descent and parking orbit trajectories have their advantages and disadvantages. A direct descent trajectory requires fewer maneuvers and typically uses less fuel. One disadvantage, however, is that the Earth departure timing Fig. 2.

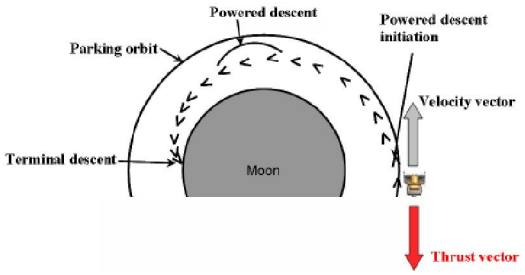

Fig. 1. Typical lunar landing scenario from parking orbit conditions.

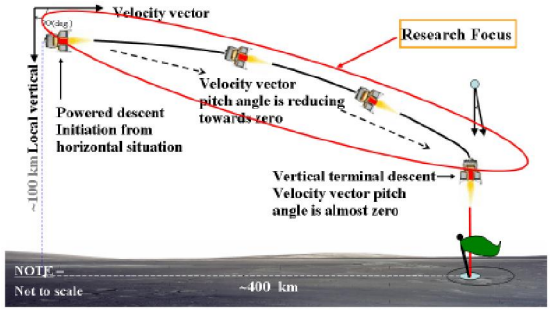

Fig. 2. Reference descent trajectory to land on Moon.

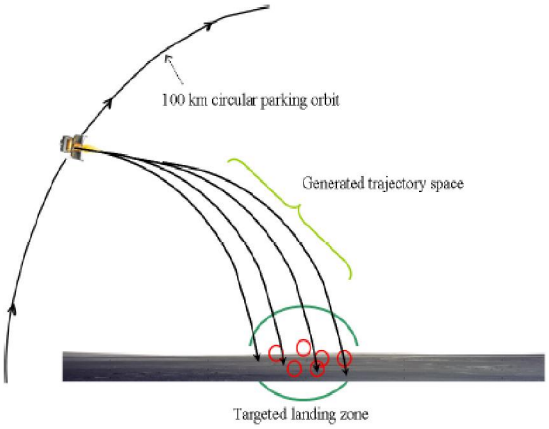

Fig. 3. Concept of trajectory space generation

Reference descent trajectory to land on Moon becomes crucial. The departure must be timed so that the vehicle not only transfers to the Moon with high accuracy, but also is in the correct position relative to the landing site at arrival. During a direct descent, there is less time to make

adjustments to the orbit or assess how much navigational error has accumulated during the Earth-Moon transfer. On the other hand, the parking orbit trajectory expends extra fuel to enter the parking orbit, but can remain in this orbit until the time of final descent. This allows time to observe landing sites, make adjustments to the orbit, perform scientific experiments, etc. The motion of the vehicle can also be observed for a longer duration of time to assess navigational error accumulation. As shown in Fig. 1 a descent from a lunar parking orbit was selected due to safety, reliability, and flexibility for this approach. The lunar descent scheme takes a horizontally oriented spacecraft from orbital speeds at a point of hundreds of kilometers from the desired landing point to an almost vertical orientation and very low speed. Figure 2 shows reference descent trajectory to land on Moon. Before it starts the powered descent, the orientation of velocity vector remains parallel to the local horizontal vector, means that, at the initiation of powered descending phase, velocity vector pitch angle is 90[deg] with respect to the local vertical axis. With the help of proposed advanced descent scheme, that will be discussed in the following Chapters, this velocity vector pitch angle will be gradually reducing towards zero during powered descent phase of lunar landing spacecraft. Consequently, at the initiation of terminal descent, velocity vector pitch angle of the lunar landing vehicle will be almost zero to ensure vertical landing, which will confirm a successful, safe pin-point landing mission.

The actual handover conditions from the orbital phase to the descent phase will be initiated close to the horizontal span and vertical range values of the desired landing site. Solution can be like that the final velocity vector pitch angle and reasonable thrust will be specified to generate a trajectory space. A desirable trajectory can then be selected from the options available. It does offer the best option for merging the handover conditions between the orbital phase termination and the descent-phase initiation in an acceptable manner. Depending on the trajectory design requirements, the trajectory space can be rather limited. Therefore, the initial and final velocity vector pitch angle, the initial and final speeds, and the gravity can also be varied to increase the trajectory space. This can be automated into an algorithm that computes a matrix of available trajectory spaces as shown in Fig. 3 and then selects the most desirable trajectory based on some user-defined criteria. Because this targeting algorithm is not iterative in nature, no risk of divergence exists in creating this trajectory space. However, the spacecraft may be at a distance that is too far from or too close to the targeted location for a safe landing, meaning that a desirable trajectory is not available. If the spacecraft is too far from the targeted landing site, the real-time guidance algorithm would wait. If the spacecraft is too close, the decision should be made to wait another orbit for the descent initiation, as shown in Fig. 4.

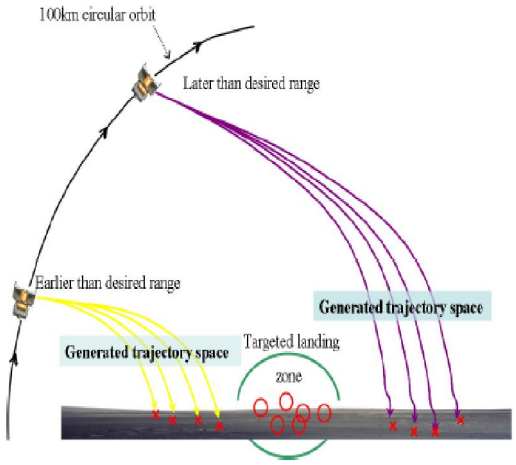

Fig. 4. Trajectory adjustment and search for a precise landing path.

3. 3 -Dimensional state equations

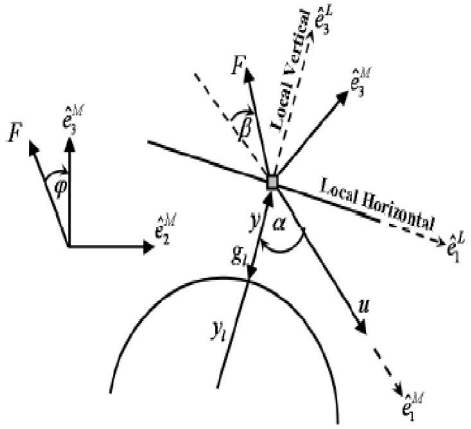

Fig. 5. Schematic diagram of lunar descent

A schematic diagram of lunar descent is described in Fig. 5. Local vertical and local horizontal (LVLH) reference frame is denoted by *L*. It also shows the relationship of the maneuver frame denoted by *M* to the LVLH unit vectors. Fundamental three dimensional equations of motion to describe the spacecraft proposition concerning a uniform sphere-shaped lunar body [Cheng (1964)] are divided into two parts. One is the equations of spacecraft motion for dynamic states as follow:

$$\dot{u}(t) = g_l cos(\alpha) - N cos(\beta). \quad (1)$$

$$\dot{\alpha}(t) = \frac{1}{u}\left[(\frac{u^2}{y+y_l} - g_l)sin\alpha - N sin\beta cos\varphi\right]. \quad (2)$$

$$\dot{\psi}(t) = \frac{1}{usin\alpha}[N sin\beta cos\varphi]. \quad (3)$$

Where u is spacecraft velocity vector magnitude or spacecraft speed, gl is lunar gravitational acceleration, N is ratio of thrust F and vehicle mass m, α is pitch angle of the vehicle velocity vector relative to the local vertical, β is angle of thrust vector relative to reverse direction of spacecraft velocity, y is altitude of the spacecraft from lunar surface, yl is lunar radius, ψ is cross range angle, and φ is thrust roll angle.

The remaining part to describe the fundamental equations of motion for kinematics states are

$$\dot{y}(t) = -ucos\alpha. \quad (4)$$

$$\dot{x}(t) = usin\alpha cos\psi \frac{y_l}{y+y_l}. \quad (5)$$

$$\dot{c}(t) = usin\alpha sin\psi \frac{y_l}{y+y_l}. \quad (6)$$

where x and c are horizontal span and cross range distance respectively.

3.1 Preliminary Postulation

Right hand sides of the spacecraft governing equations are reduced to function of velocity vector pitch angle α. For this purpose some reasonable assumptions are made regarding thrust to mass ratio, thrust vector angle and lunar gravitational acceleration force. To generate an ideal descent trajectory it is rational to assume a constant value for N i.e., F/m and g_l, and control input β is set to zero. But in the situation of constant thrust acceleration, m will not be constant and so F/m is varying. Yet, this error will be removed by the real time guidance algorithm. Therefore, using initial values for mass and gravity is a straightforward assumption for this solution. The changes are observed bellow:

$$\dot{\alpha}(t) = \frac{1}{u}[(\frac{u^2}{y+y_l} - g_l)\sin\alpha] \quad (7)$$

$$\dot{u}(t) = g_l \cos\alpha - N \quad (8)$$

$$\dot{\psi}(t) = 0 \quad (9)$$

Therefore, $\psi(t)$ is constant. Hear we can take some assumption at the face of reference trajectory generation.

It is reasonable to assume that $y << y_l$ in order that $y_l/y + y_l \approx 1$. Then the equation for down range and cross range become

$$\dot{x}(t) = u\sin\alpha\cos\psi \quad (10)$$

$$\dot{c}(t) = u\sin\alpha\sin\psi \quad (11)$$

4. 3 -dimensional inclusive numerical resolutions

To find the full integrated numerical solutions for speed u, time t, downrange x, altitude y and cross range c as a function of velocity vector pitch angle α during power descend phase; authors have performed the following mathematical derivations for simplification. Therefore, the equation for speed is derived with the help of Eq. (7) and Eq. (8).

$$\dot{u}(\alpha) = \frac{\frac{du}{dt}}{\frac{d\alpha}{dt}} = \frac{u(g_l\cos\alpha - N)}{\frac{1}{u}(\frac{u^2}{y_l} - g_l)\sin\alpha} \quad (12)$$

or

$$\frac{1}{u}(\frac{u^2}{y_l} - g_l)du = \frac{g_l cos\alpha - N}{sin\alpha}d\alpha,$$

which can be integrated as

$$\int_{u_0}^{u} \frac{1}{u}(\frac{u^2}{y_l} - g_l)du = \int_{\alpha_0}^{\alpha} \frac{g_l cos\alpha - N}{sin\alpha}d\alpha,$$

Therefore,

$$\dot{u}(\alpha) = [-g_l y_l W]^{\frac{1}{2}}, \quad (13)$$

where Lambert function W is expressed as

$$W = -\frac{u_0^2}{g_l y_l}\frac{\sin\alpha^{-2}}{e^{(\frac{u_0^2}{g_l y_l})}}\left(\frac{1+\cos\alpha}{\sin\alpha}\right)^{-\frac{2N}{g_l}} \quad (14)$$

Now the inclusive numerical resolution for descent time, t_D as a function of velocity vector pitch angle, α can be obtained by integrating the following equation developed by Eq. (8) and Eq. (12)

$$\dot{t}_D(\alpha) = \frac{dt_D}{d\alpha} = \frac{\frac{du}{d\alpha}}{\frac{du}{dt_D}} = \frac{\dot{u}(\alpha)}{\dot{u}(t)}, \quad (15)$$

Again for altitude and down range, it can be written that

$$\dot{y}(\alpha) = \frac{dy}{d\alpha} = \frac{dy}{dt_D}\frac{dt_D}{d\alpha} = \dot{y}(t)\dot{t}_D(\alpha) \quad (16)$$

now substituting the values from equations (4)

$$\dot{y}(\alpha) = -u\cos\alpha\dot{t}_D(\alpha), \quad (17)$$

where u can be replaced from equation (13). For the solution of horizontal span as a function of velocity vector pitch angle α, the same procedure can be followed.

$$\dot{x}(\alpha) = \frac{dx}{d\alpha} = \frac{dx}{dt_D}\frac{dt_D}{d\alpha} = \dot{x}(t)\dot{t}_D(\alpha) \quad (18)$$

now from equation (10)

$$\dot{x}(\alpha) = u\sin\alpha\cos\psi\dot{t}_D(\alpha). \quad (19)$$

and similar procedure is applied for the derivation of cross range

$$\dot{c}(\alpha) = u\sin\alpha\sin\psi\dot{t}_D(\alpha). \quad (20)$$

5. 3 –D Conventional descent solution

Analytical solution for lunar descent is obtained here by assuming the lunar surface as a plane surface so that the lunar radias yl → ∞ so that equation (7) now reduces to:

$$\dot{\alpha}(t) = -\frac{g_l}{u}\sin\alpha \quad (21)$$

This reduced equation is used to obtain a single, distinguishable differential equation with α as the self-regulating variable. From the above we have:

$$\dot{u}(\alpha) = \dot{u}(t)/\dot{\alpha}(t) = -\frac{u(g_l\cos\alpha - N)}{g_l\sin\alpha} \quad (22)$$

then

$$\frac{1}{u}\frac{du}{d\alpha} + \frac{\cos\alpha}{\sin\alpha} - \frac{N}{g_l}\frac{1}{\sin\alpha} = 0 \quad (23)$$

Now Eq. (23) can be integrated to obtain the descent speed u as a function of velocity vector pitch angle α as [1,3]:

$$u(\alpha) = u_0\left[\frac{\sin\alpha_0}{\sin\alpha}\right]\left[\frac{\tan(\alpha/2)}{\tan(\alpha_0/2)}\right]^{\frac{N}{g_l}} \quad (24)$$

where, u0 and α0 are initial values for speed and velocity vector pitch angle respectively.

Differentiating Eq. (24):

$$\dot{u}(\alpha) = \frac{du}{d\alpha} = u_0\left[\frac{\sin\alpha_0}{\sin\alpha}\right]\left[\frac{\tan(\alpha/2)}{\tan(\alpha_0/2)}\right]^{\frac{N}{g_l}}\left[\frac{N}{g_l\sin(\alpha)} - \cot\alpha\right] \quad (25)$$

Using the above value of the speed u, we can obtain the solution for time, altitude, down range and cross range. First, the descent time is given as:

$$\dot{t}_D(\alpha) = \frac{dt_D}{d\alpha} = \frac{du}{d\alpha}\Big/\frac{du}{dt_D} \quad (26)$$

Using equations (8) and (25) gives:

$$\dot{t}_D(\alpha) = u_0\left[\frac{\sin\alpha_0}{\sin\alpha}\right]\left[\frac{\tan(\alpha/2)}{\tan(\alpha_0/2)}\right]^{\frac{N}{g_l}}\left[\frac{N}{g_l\sin(\alpha)} - \cot\alpha\right]\left[\frac{1}{g_l\cos\alpha - N}\right] \quad (27)$$

Similarly, the altitude is given as:

$$\dot{y}(\alpha) = \frac{dy}{d\alpha} = \frac{dy}{dt_D}\Big/\frac{d\alpha}{dt_D} \quad (28)$$

Using equations (4), (21) and (25) gives:

$$\dot{y}(\alpha) = \frac{u^2}{g_l}\cot\alpha = u_0^2\left[\frac{\sin\alpha_0}{\sin\alpha}\right]^2\left[\frac{\tan(\alpha/2)}{\tan(\alpha_0/2)}\right]^{\frac{2N}{g_l}}\left[\frac{\cot\alpha}{g_l}\right] \quad (29)$$

Using equations (10) and (21), the down range distance is given as:

$$\dot{x}(\alpha) = \frac{dx}{dt_D}\Big/\frac{d\alpha}{dt_D} = -\frac{u^2}{g_l}\cos\psi \quad (30)$$

Using equations (25) gives:

$$\dot{x}(\alpha) = -u_0^2\left[\frac{\sin\alpha_0}{\sin\alpha}\right]^2\left[\frac{\tan(\alpha/2)}{\tan(\alpha_0/2)}\right]^{\frac{2N}{g_l}}\left[\frac{1}{g_l}\right]\cos\psi \quad (31)$$

Similarly, using equations (11) and (21), the cross range distance is given as:

$$\dot{c}(\alpha) = \frac{dc}{dt_D}\Big/\frac{d\alpha}{dt_D} = -\frac{u^2}{g_l}\sin\psi \quad (32)$$

Using equations (25) gives:

$$\dot{c}(\alpha) = -u_0^2\left[\frac{\sin\alpha_0}{\sin\alpha}\right]^2\left[\frac{\tan(\alpha/2)}{\tan(\alpha_0/2)}\right]^{\frac{2N}{g_l}}\left[\frac{1}{g_l}\right]\sin\psi \quad (33)$$

5.1. Descent constraints

Along with the assumptions described in Section 3.1, other required descent specifications are considered to integrate the developed equations and to compare the simulation results between numerical solution and analytical solution for lunar descent scheme. Specific descent speculations are shown in Table 1.

Table 1. Lunar descent specification

Lunar descent specification	
Lunar gravitational acceleration (gl)	1.623 [m/s 2]
Thrust to mass ratio (N)	4 [N/kg]
Initial lander speed (u0)	1688 [m/s]
Initial velocity vector pitch angle (α0)	90 [deg]
Initial altitude for powered descent	100 [km]

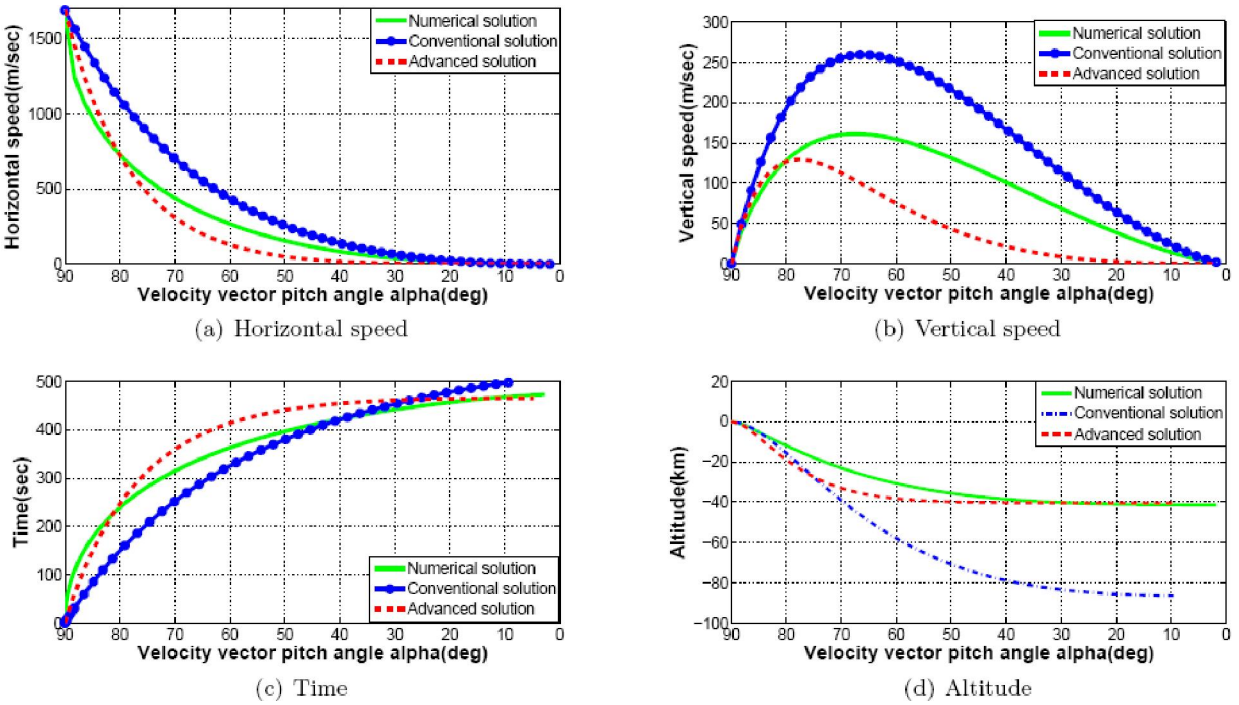

Fig. 6. Comparison between numerical solution, convention analytical solution and proposed advanced analytical solution: Speed, time and altitude

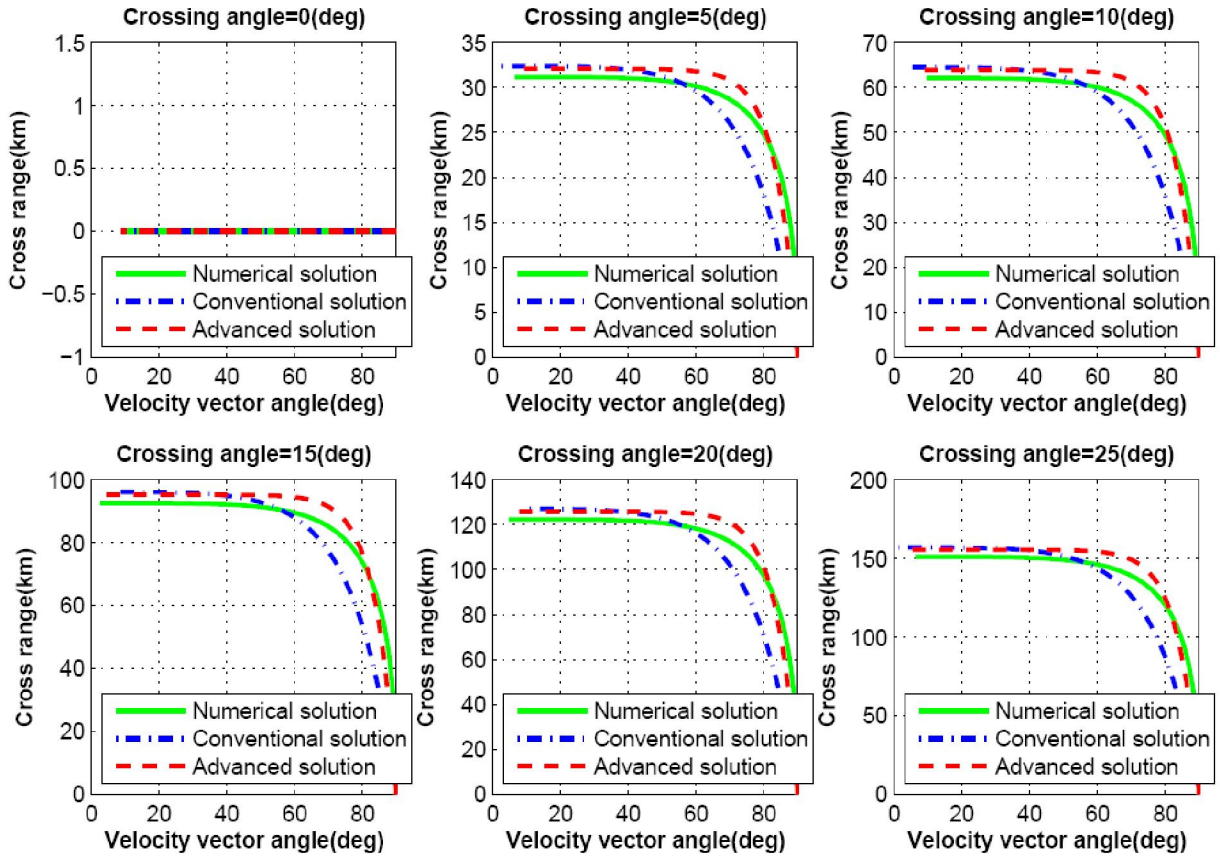

Fig. 7. Cross range response varying crossing angle from 0.0 degree to 25 degree.

6. 3-Dimensional advanced lunar descent solution

To solve the same governing equations for the proposed 3-dimensional advanced scheme, it is again necessary that the right hand sides of the equations are kept as a function of velocity vector pitch angle α. New assumption of centrifugal acceleration term is considered for homogeneous spherical lunar surface. Assumptions for mass and lunar gravity are identical to the Section 3.1. But for centrifugal acceleration term, a constant value Γ can be logically chosen which is defined as the ratio between centrifugal acceleration and lunar gravitational acceleration. Though this is noticeably a varying value, during reference trajectory generation phase it is reasonable to consider as an assumption at the initial stage because the real-time guidance will compensate for the errors between the model and the environment. Therefore,

$$\Gamma = \frac{u^2}{y + y_l} \Big/ g_l \qquad (34)$$

$$\frac{u^2}{y + y_l} - g_l = -(1-\Gamma) g_l \qquad (35)$$

6.1 Mathematical Derivation

With these assumptions and making consistent with the traditional lunar descent works, [Cheng (1964), McInnes (1999), and McInnes (2003)] speed can be recognized by following differential equations formulating as a function of velocity vector pitch angle α.

$$\dot{u}(\alpha) = \dot{u}(t)/\dot{\alpha}(t) = u \frac{g_l \cos\alpha - N}{-(1-\Gamma) g_l \sin\alpha} \qquad (36)$$

then

$$\frac{du}{u} = \left[\frac{g_l \cos\alpha - N}{-(1-\Gamma) g_l \sin\alpha}\right] d\alpha \qquad (37)$$

This equation can now be directly integrated to obtain the descent velocity u as a function of the velocity vector pitch angle α as

$$u(\alpha) = u_0 e^{\int_{\alpha_0}^{\alpha} \left[\frac{g_l \cos\alpha - N}{-(1-\Gamma) g_l \sin\alpha}\right] d\alpha} \qquad (38)$$

Now

$$\int_{\alpha_0}^{\alpha} \left[\frac{g_l \cos\alpha - N}{-(1-\Gamma) g_l \sin\alpha}\right] d\alpha = ln\left[\frac{\sin\alpha}{\sin\alpha_0}\right]^{\frac{-1}{(1-\Gamma)}} + ln\left[\frac{\tan\frac{\alpha_0}{2}}{\tan\frac{\alpha}{2}}\right]^{\frac{-N}{(1-\Gamma) g_l}} \qquad (39)$$

Therefore,

$$u(\alpha) = u_0 \left[\frac{\sin\alpha}{\sin\alpha_0}\right]^{\frac{-1}{(1-\Gamma)}} \left[\frac{\tan\frac{\alpha_0}{2}}{\tan\frac{\alpha}{2}}\right]^{\frac{-N}{(1-\Gamma) g_l}} \qquad (40)$$

as $tan(\frac{\alpha}{2}) = \frac{1-\cos\alpha}{\sin\alpha}$ and let that $\tau = \frac{1}{1-\Gamma}$ & $\rho = \frac{N}{g_l}$. Where $\rho > 0$ in order that

$$u(\alpha) = u_0 \left[\frac{\sin\alpha}{\sin\alpha_0}\right]^{-\tau} \left[\frac{\frac{1-\cos\alpha_0}{\sin\alpha_0}}{\frac{1-\cos\alpha}{\sin\alpha}}\right]^{-\tau\rho} \qquad (41)$$

where $\tau = 1/(1-\Gamma)$ is a measure of the centrifugal acceleration term. Then, the solution for current speed obtains the shape:

$$u(\alpha) = u_0 \left(\frac{\sin\alpha}{\sin\alpha_0}\right)^{-\tau(1+\rho)} \left(\frac{1-\cos\alpha_0}{1-\cos\alpha}\right)^{-\tau\rho} \qquad (42)$$

Now the descent time t_D, vertical range $y(\alpha)$ and horizontal span $x(\alpha)$ are resolved in an identical manner of the conventional gravity turn descent solution as follow

$$\dot{t}_D(\alpha) = 1/\dot{\alpha}(t) = \frac{-\tau u(\alpha)}{g_l \sin\alpha} = \frac{-\tau u_0}{g_l} \frac{(1-\cos\alpha_0)^{-\tau\rho}}{(\sin\alpha_0)^{-\tau(1+\rho)}} \frac{(\sin\alpha)^{-\tau(1+\rho)-1}}{(1-\cos\alpha)^{-\tau\rho}} \qquad (43)$$

$$\dot{t}_D(\alpha) = G_{t_D} \frac{(\sin\alpha)^{-\tau(1+\rho)-1}}{(1-\cos\alpha)^{-\tau\rho}}, \qquad (44)$$

where $G_{t_D} = \frac{-\tau u_0}{g_l} \frac{(1-\cos\alpha_0)^{-\tau\rho}}{(\sin\alpha_0)^{-\tau(1+\rho)}}$ (45)

Now for altitude,

$$\dot{y}(\alpha) = \frac{\dot{y}(t)}{\dot{\alpha}(t)} = \frac{\tau u_0^2}{g_l} \frac{(1-\cos\alpha_0)^{-2\tau\rho}}{(\sin\alpha_0)^{-2\tau(1+\rho)}} \frac{(\sin\alpha)^{-2\tau(1+\rho)} \cos\alpha}{(1-\cos\alpha)^{-2\tau\rho} \sin\alpha} \qquad (46)$$

$$\dot{y}(\alpha) = G_y \frac{(\sin\alpha)^{-2\tau(1+\rho)-1} \cos\alpha}{(1-\cos\alpha)^{-2\tau\rho}} \qquad (47)$$

$$G_y = \frac{\tau u_0^2}{g_l} \frac{(1-\cos\alpha_0)^{-2\tau\rho}}{(\sin\alpha_0)^{-2\tau(1+\rho)}} \qquad (48)$$

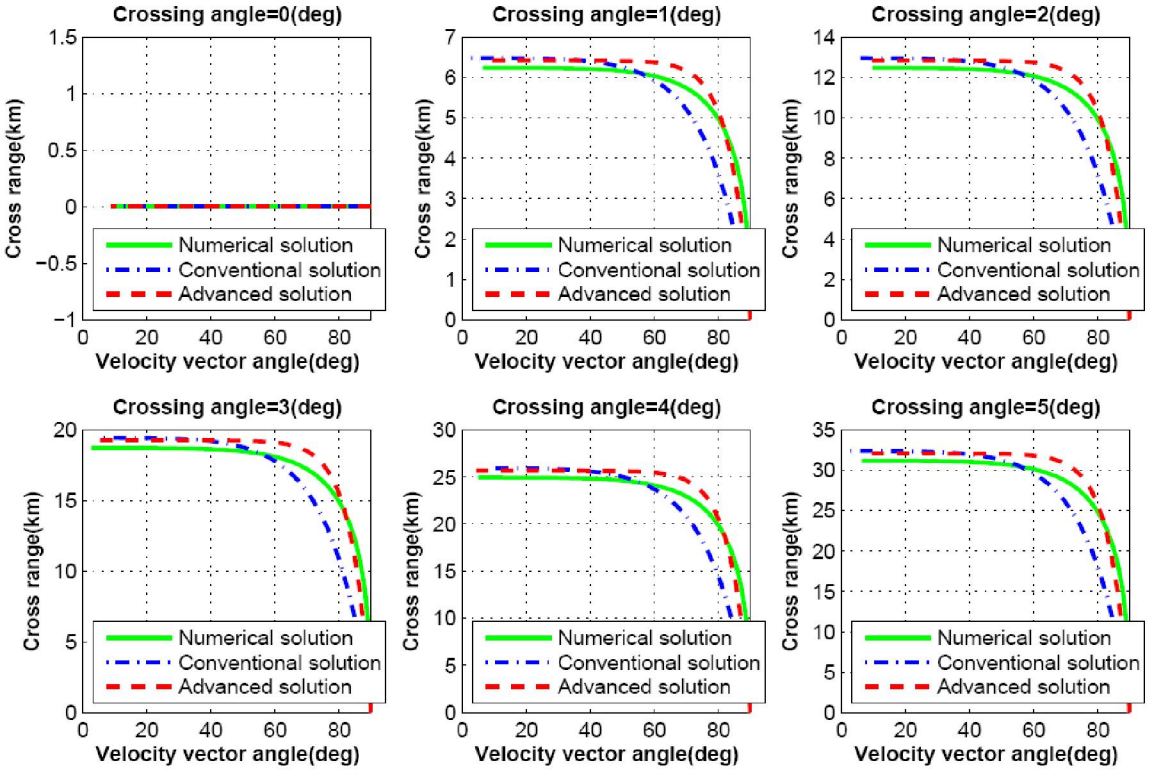

Fig. 8. Cross range response varying crossing angle from 0.0 degree to 05 degree

Now for downrange,

$$\dot{x}(\alpha) = \frac{\dot{x}(t)}{\dot{\alpha}(t)} = \frac{-\tau u_0^2}{g_l}\frac{(1-\cos\alpha_0)^{-2\tau\rho}}{(\sin\alpha_0)^{-2\tau(1+\rho)}}\cos\psi \frac{(\sin\alpha)^{-2\tau(1+\rho)}}{(1-\cos\alpha)^{-2\tau\rho}} \quad (49)$$

$$\dot{x}(\alpha) = G_x\frac{(\sin\alpha)^{-2\tau(1+\rho)}}{(1-\cos\alpha)^{-2\tau\rho}}\cos\psi \quad (50)$$

where

$$G_x = \frac{-\tau u_0^2}{g_l}\frac{(1-\cos\alpha_0)^{-2\tau\rho}}{(\sin\alpha_0)^{-2\tau(1+\rho)}} \quad (51)$$

and the cross range,

$$\dot{c}(\alpha) = \frac{\dot{c}(t)}{\dot{\alpha}(t)} = \frac{-\tau u_0^2}{g_l}\frac{(1-\cos\alpha_0)^{-2\tau\rho}}{(\sin\alpha_0)^{-2\tau(1+\rho)}}\sin\psi \frac{(\sin\alpha)^{-2\tau(1+\rho)}}{(1-\cos\alpha)^{-2\tau\rho}} \quad (52)$$

$$\dot{c}(\alpha) = G_c\frac{(\sin\alpha)^{-2\tau(1+\rho)}}{(1-\cos\alpha)^{-2\tau\rho}}\sin\psi \quad (53)$$

where,

$$G_c = \frac{-\tau u_0^2}{g_l}\frac{(1-\cos\alpha_0)^{-2\tau\rho}}{(\sin\alpha_0)^{-2\tau(1+\rho)}} \quad (54)$$

It is evoked that the τ is the measure of the relation between centrifugal acceleration and lunar gravitational acceleration terms. With the purpose of integration for above equations in a qualitative manner the value for τ must be an integer. This entails τ = 1, 2, 3, 4 . . . . . Instead of this solution, directly the ratio Γ, which is mentioned earlier, can be chosen some fractional values to make τ an integer. But the authors found better results having directly the integer logical values to get a qualitative integration of these equations. Choosing a logical value directly for the τ proves more preciseness in approximation as well. The influences of differing the constant τ is demonstrated in previous work[Mehedi and Kubota (2011)]. Unlike values (1, 2, 3, 4, 5, ...) for τ are employed into equations (42), (44), (47), (50) and (53) and these equations are numerically integrated with constant approximate values for g_l and N whereas g_l =1.623 *m/sec*^{2} and N = 5 *N/kg*. Initial and final values for the velocity vector pitch angle α is taken 90^0 and 0^0 while the initial speed $u0$ is considered as approximate orbital speed, 1688 *m/sec*. In contrast of this advanced solution, full numerical integrated resolution to equations (1), (2), (4), (5) and (6), and traditional gravity-turn solutions to equations [Cheng (1964); McInnes (1999, 2003)] are performed for comparison taking same approximation for β,gl,N,α and $u0$ as it is made into equations (42), (44), (47), (50) and (53) while no estimation are made about the centrifugal acceleration.

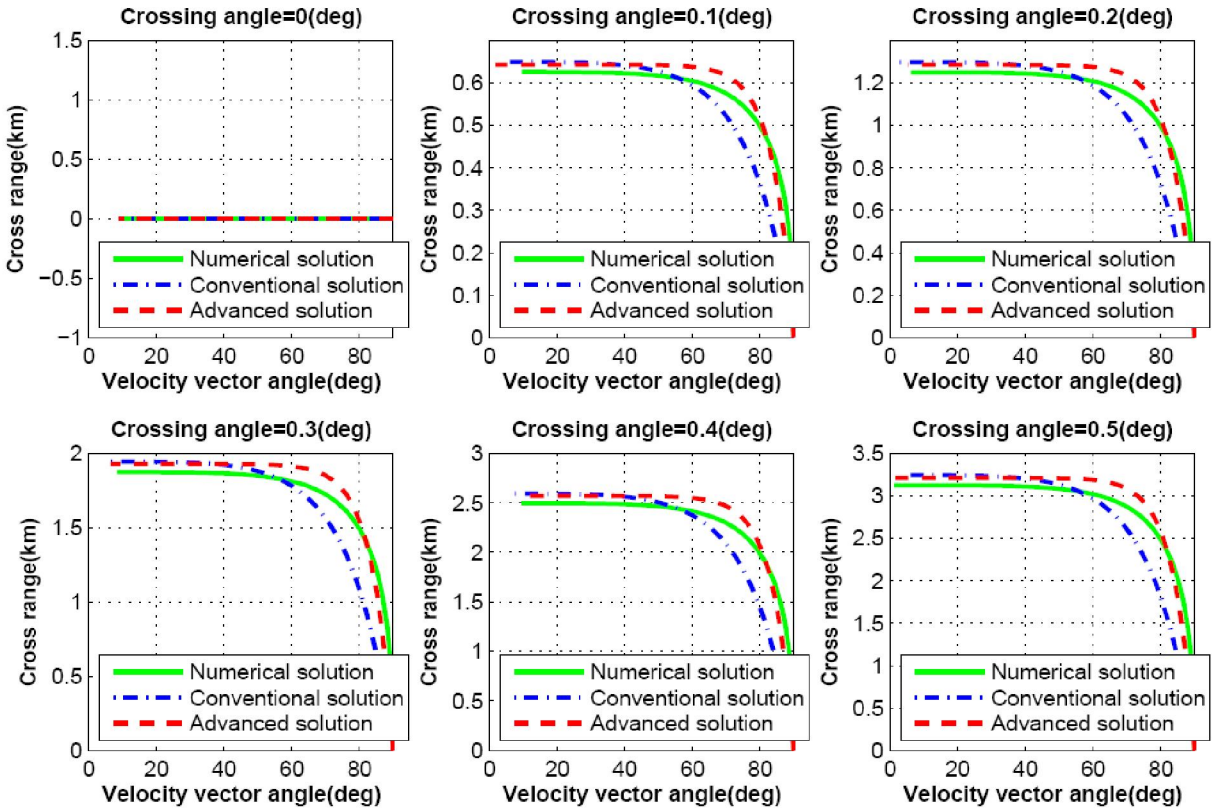

Fig. 9. Cross range response varying crossing angle from 0.0 degree to 0.5 degree

A comprehensive evaluation of this advanced solution with traditional gravity-turn solution, and a numerically integrated solution to the full equations of lunar module descent are exposed in this investigation. It can be noted that varying τ has reasonable impact on different responses for speed, time, vertical range and horizontal span for lunar descent scheme. The largest impact is observed on the final vertical range variation. The centrifugal acceleration effectively adjusts the rate of change of the vehicle velocity vector pitch angle which impacts the direction of the velocity vector. Therefore, the term τ directly influences the vertical range of the trajectory. From the assessment of the various values for τ, a value of $\tau = 2$ emerges to be a realistic number and improves on different responses of advanced solutions for speed, time, vertical range and horizontal span over traditional solutions.

7. Simulation results

It is observed in the previously derived equations that there is no effect of crossing angle, ψ on the equations for speeds, time and altitude. Therefore, different trajectory responses for descent speeds, time and altitude are shown in as shown in Figs. 6(a), 6(b), 6(c) and 6(d). as a comparison between numerical, conventional and advanced analytical descent illumination given $\tau = 2$ to the fully integrated solutions to equations (1), (2), (4) and (5) where $\beta = 0$. The fully integrated solution assumes a constant lunar gravitational acceleration, g_l, and constant thrust to mass ratio, N, but does not guess a constant centrifugal acceleration. The computer simulation results for full integrated solution is considered as an ideal measure of lunar descent trajectory. But the method is complex and iterative. It needs long time to execute and not suitable for real time application. However, the result of this ideal situation is a model to follow by any type of solution. It is pleasing if it would get responses with a miniature divergence between a new solution and ideal numerical solution and better performance than the conventional one. For this purpose and advanced analytical solution is proposed here and compared the responses. In the Figs. 6(a), 6(b), and 6(c), speed and time responses are almost similar between numerical, conventional and advanced analytical solution. Great impact is observed for altitude response in Fig. 6(d) which demonstrates the trajectory discrepancy and the guidance will be required to remove.

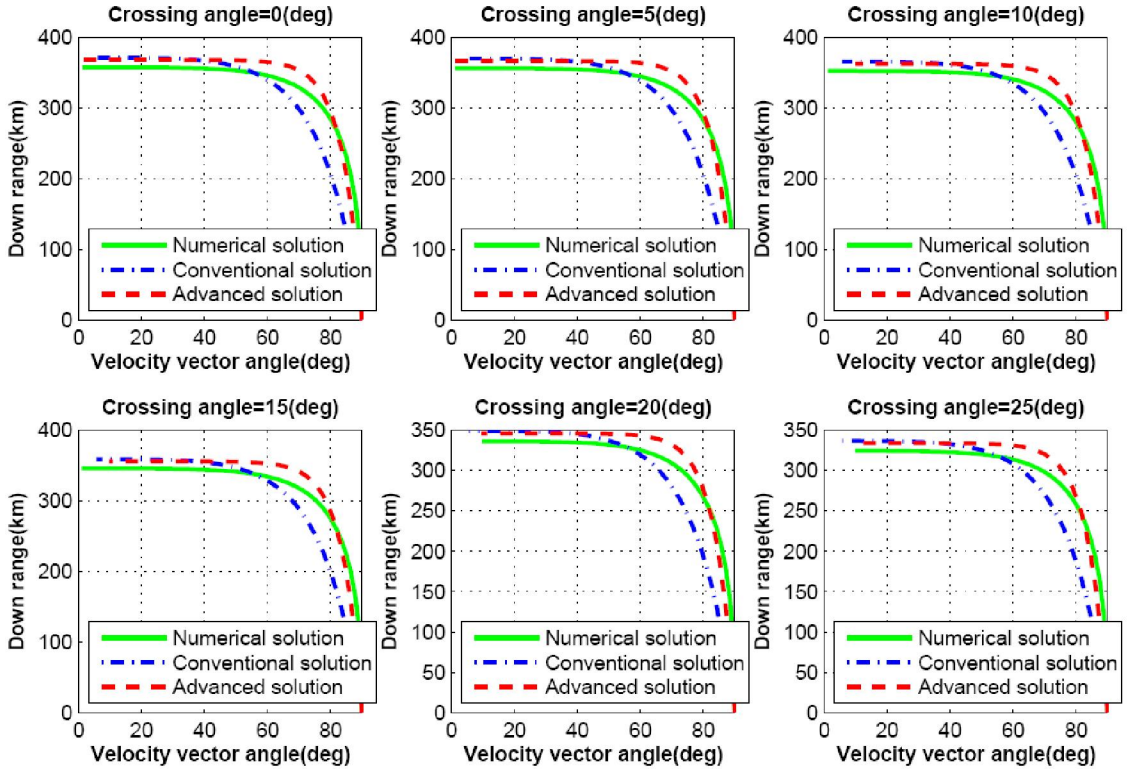

Fig. 10. Downrange response varying crossing angle from 0.0 degree to 25 degree

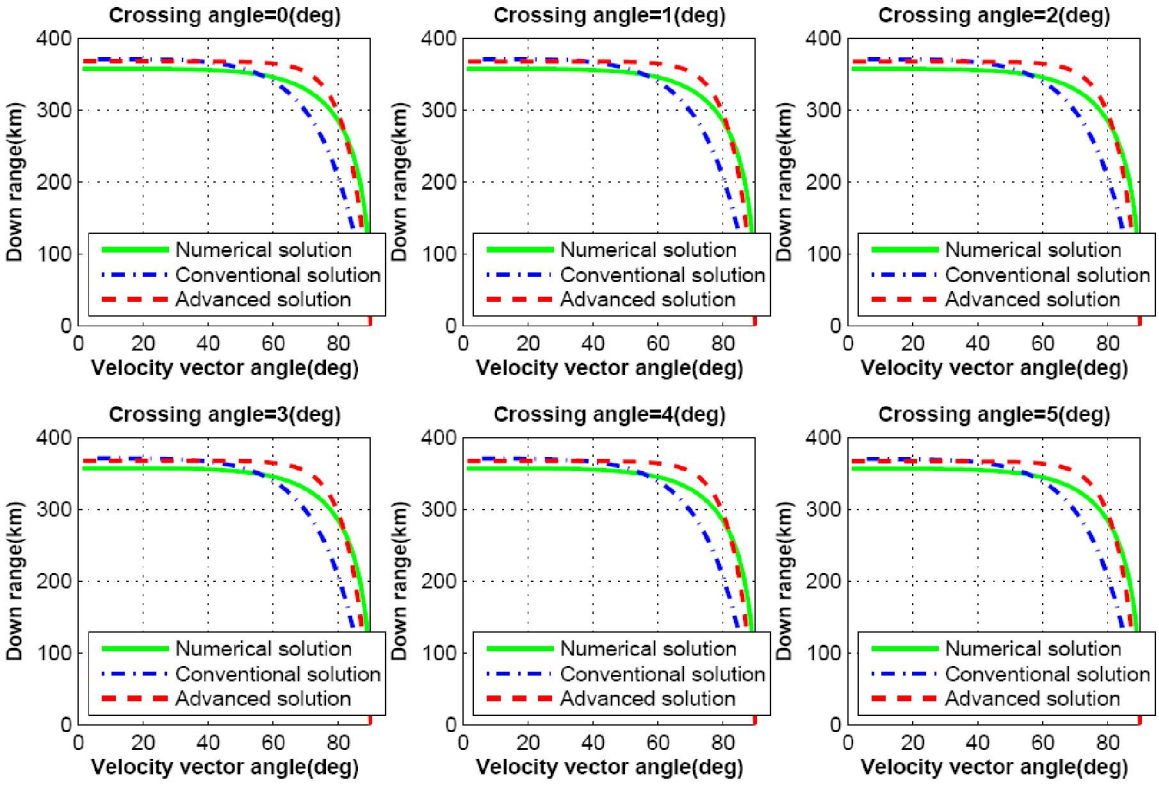

Fig. 11. Downrange response varying crossing angle from 0.0 degree to 5 degree

Figures 7, 8, and 9 show simulation results for cross range responses of both numerical, conventional and advanced analytical solutions as a function of velocity vector pitch angle. Crossing angle is a major factor for variation of cross range distance. Authors varied the crossing angle intentionally to observe the effect on cross range distance during lunar descent. Lunar landing spacecraft does not travel towards cross range distance while the crossing angle is maintained zero degree. With the variation of crossing angle between zero degree to 25 degree, spacecraft travels more than 150 km far towards cross range as shown in Fig. 7. If the crossing angle is maintained within 5 degree, spacecraft moves with in the range of 32.5 km. Deviation of cross range distance per degree is shown in Fig. 8.

Crossing angle is an important factor for precise lunar landing mission. In previous approaches lunar descent trajectory is designed assuming that the crossing angle is zero. But the simulation results shown in Fig. 9 that, lunar landing spacecraft deviates more than 600 m from the line of down range while crossing angle is changed from zero to 0.1 degree. For 0.5 degree of crossing angle spacecraft moves more than 3 km from the line of down range.

Above analysis proves that the crossing angle plays a major role in trajectory design for precise lunar landing mission. Further, only the cross range distance is not affected with the change of crossing angle, it influences the down range range distance as well. Figs. 10 and 11 show the simulation results for down range response of both numerical, conventional and advanced solutions as a function of velocity vector pitch angle. With the increase of crossing angle, down range distance decrease. As a result, lunar landing spacecraft will travel shorter distance than the required. If the crossing angle increase up to 25 degree, down range distance decreases more than 30 km as shown in Fig. 10. The influence on down range due to the change of each degree crossing angle is shown in Fig. 11.

It is already mentioned that the advanced solutions are presented to reduce the complexity of numerical solution and to overcome the limitations of conventional scheme. Cross range and down range responses of above simulation results prove that the deviation occurs between numerical conventional and advanced solution. These deviation will influence on precise lunar landing mission. Again, advanced solution of lunar descent motion equation is much more suitable for real-time application. Deviation of cross range and down range from ideal solution can be overcome using real-time guidance scheme during descent.

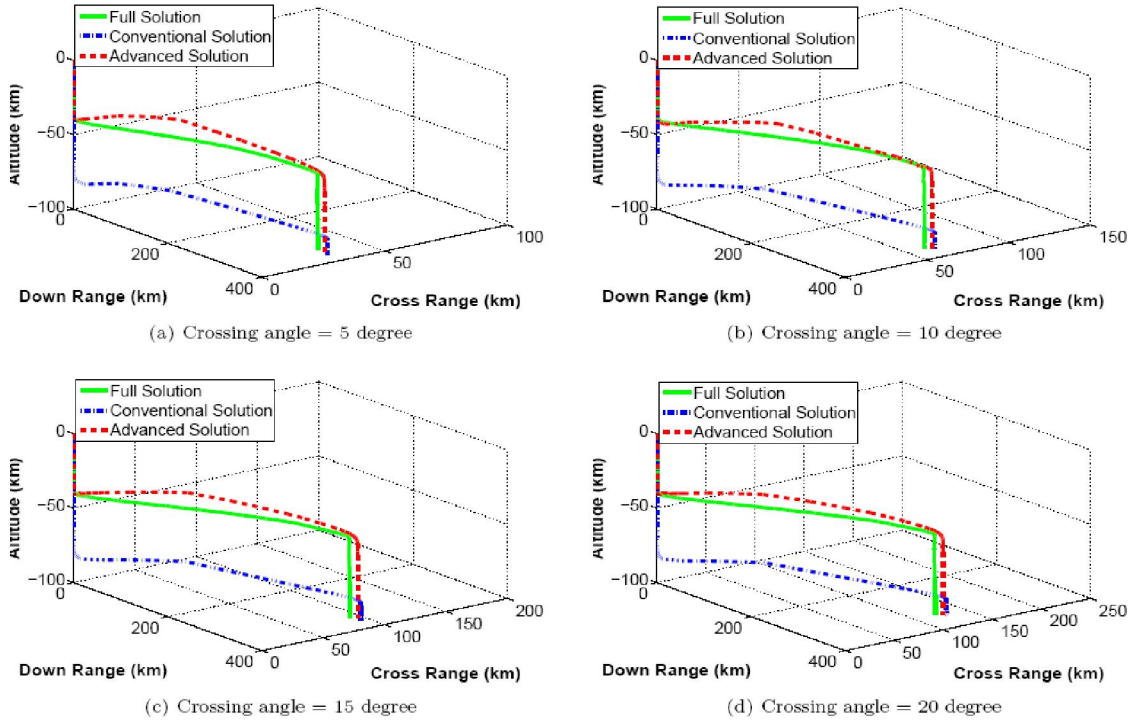

(a) Crossing angle = 5 degree

(b) Crossing angle = 10 degree

(c) Crossing angle = 15 degree

(d) Crossing angle = 20 degree

Fig. 12. 3-dimensionalflightpathcomparisonbetweennumericalandanalyticalsolutionfordifferentcrossingangle

8. 3-Dimensional response

Section 4, 5 and 6 described the detail mathematical modeling of 3-dimensional representation for numerical conventional and advanced descent solution of lunar landing mission. Based on that derivation, computer simulation is performed. Figure 12(a), 12(b), 12(c) and 12(d) represents a comparison of 3-dimensional trajectory responses for spacecraft descent on lunar surface while the governing equations are solved by complete integration method, conventional illumination and advanced solution scheme. Equations of different states are numerically integrated with the constant values for lunar gravitational acceleration g_l, thrust to mass ratio N , initial vehicle speed u_0 and initial velocity vector pitch angle α_0 mentioned in Table 1. Simulation is categorized for different values of crossing angle between 5 degree to 20 degree with the increment of 5 degree. It is observed that, altitude is not affected at all, while crossing angle is changing. On the other hand, down range and cross range distances are influenced because of different values of crossing angle. Result shows that the trajectory response of less complex advanced solution is always following the response of ideal but complex numerical solution
having better performance than the conventional method of solution.

9. Conclusion

The conventional 2-dimensional lunar descent and landing problem has been advanced to allow an accurate representation of lunar descent from orbital condition. A comprehensive 3-dimensional evaluation of advanced scheme, conventional illumination and numerical solution for lunar landing spacecraft is exposed in this investigation Finding a reasonable assumption for lunar surface and centrifugal acceleration, it significantly advanced the sphere of validity of the traditional gravity-turn solution from low velocity terminal descent to a complete descent from orbital situation. The accessibility of the descent velocities, time, vertical range and horizontal span as a function of the velocity vector pitch angle could be utilized to lessen the computational trouble on real-time lunar descent guidance scheme for future landing mission.

Acknowledgements:

This article was funded by the Deanship of Scientific Research (DSR), King Abdulaziz University, Jeddah. The authors, therefore, acknowledge with thanks DSR technical and financial support. It was also supported by the facility of Japan Aerospace Exploration Agency (JAXA).

Corresponding Author:
Dr. Ibrahim Mustafa Mehedi
Department of ECE
King Abdulaziz University
Jeddah, Saudi Arabia
E-mail: imehedi@kau.edu.sa

References

1. Acikmese, B. and Blackmore, L. (2011). Lossless convexication for a class of optimal control problems with nonconvex control constraints. *Automatica*, 47(2), 341– 347.
2. Ackmese, B. and Polen, S. (2007). A convex programming approach to constrained powered descent guidance for mars pinpoint landing. *AIAA Journal of Guidance, Control and Dynamics*, 30(5), 1353–1366.
3. Blackmore, L., Acikmese, B., and Scharf, D. (2010). Minimum landing-error powered descent guidance for mars landing using convex optimization. *AIAA Journal of Guidance, Control and Dynamics*, 33(4), 1161–1171.
4. Braun, R. and Manning, R. (2007). Mars exploration entry, descent and landing challenges. *Journal of Spacecraft and Rockets*, 44(2), 10–323.
5. Cheng, R. (1964). Lunar terminal guidance. In *Lunar Missions and Exploration, edited by C. T. Leondes and R. W. Vance, Univ. of California Engineering and Physical Sciences Extension Series*, 308–355. Wiley, New York.
6. Cheng, R., Meredith, C., and Conrad, D. (1966). Design considerations for surveyor guidance. *Journal of Spacecraft and Rockets*, 3(11), 1569–1576.
7. Chomel, C. and Bishop, R. (2009). Analytical lunar descenr guidance algorithm. *Journal of Guidance, Control and Dynamics*, 32(3), 915–926.
8. Kenji, U., Yuzo, S., and Shingo, N. (2002). Tracking control to near-optimal trajectory for a lunar lander. *23rd International Symposium on Space Technology and Science*, 1, 977–982.
9. Klumpp, R. (1971). Apollo guidance, navigation, and control: Apollo lunar-descent guidance. Technical report, MIT Charles Stark Draper Laboratory.
10. Klumpp, R. (1974). Apollo lunar descent guidance. *Automatica*, 10(2), 133–146.
11. Lutz, T. (2010). Application of auto-rotation for entry, descent and landing on mars. *7th*

International Planetary Probe Workshop.
12. Mattingley, J. and Boyd, S. (2010). Real-time convex optimization in signal processing. *IEEE Signal Processing Magazine*, 3(11), 1569–1576.
13. McInnes, C. (2003). Gravity-turn descent from low circular orbit conditions. *Journal of Guidance Control and Dynamics*, 26(1), 183–185.
14. Mehedi, I. and Kubota, T. (2011). Advanced guidance scheme for lunar descent and landing from orbital speed conditions. *Transaction of Japan Society for Aeronautical and Space Sciences*, 54(184), 98–105.
15. Najson, F. and Mease, K. (2006). Computationally inexpensive guidance algorithm for fuel-efficient terminal descent. *Journal of Guidance, Control and Dynamics*, 29(4), 955–964.
16. Sostaric, R. (2006). Lunar descent reference trajectory. Technical report, NASA/JSC.
17. Steinfeld, B., Grant, M., Matz, D., Braun, R., and Barton,
18. G. (2010). Guidance, navigation and control system performance trades for mars pinpoint landing. *AIAA Journal of Spacecraft and Rockets*, 47(1).
19. Sturm, J.F. (2002). Implementation of interior point methods for mixed semidefinite and second order cone optimization problems. *Optimization Methods and Software*, 17(6), 1105–1154.
20. Sturm, J. (1999). A matlab toolbox for optimization over symmetric cones. *Optimization Methods and Software*, 11(1), 625–635.
21. Topcu, U., Casoliva, J., and Mease, K. (2007). Minimum-fuel powered descent for mars pinpoint landing. *Journal of Spacecraft and Rockets*, 44(2), 324–331.
22. Ueno, S. and Yamaguchi, Y. (1998). Near-minimum guidance law of a lunar landing module. *14th IFAC Symposium on Automatic Control in Aerospace*, 377– 382.
23. Xing-Long, L., Gaung-Ren, D., and Kok-Lay, T. (2008). Optimal soft landing control for moon lander. *Automatica*, 44, 1097–1103.
24. Ye, Y. (1997). *Interior Point Algorithms*, volume 33. Wiley, New York.

2/15/2021